Journal of Hazardous Materials 507 (2026) 141833

Contents lists available at ScienceDirect

Journal of Hazardous Materials

journal homepage: www.elsevier.com/locate/jhazmat

Robust decomplexation of Cu(II) complexes in excessive ligand environments by Mn(II)/PMS process: Ligand concentration-dependent decomplexation mechanisms

Zhe Xu [a,b,1,*], Weilan Zhen [b,1], Chengfeng Liu [b], Jiantong Zhou [b], Taicheng An [a,b]

[a] Guangdong Key Laboratory of Environmental Catalysis and Health Risk Control, Guangdong-Hong Kong-Macao Joint Laboratory for Contaminants Exposure and Health, Institute of Environmental Health and Pollution Control, Guangdong University of Technology, Guangzhou 510006, China
[b] School of Environmental Science and Engineering, Guangdong University of Technology, Guangzhou 510006, China

HIGHLIGHTS

- Cu(II) complexes with ligand excess were effectively decomplexed by Mn (II)/PMS process.
- Influence of operational parameters was systematically evaluated.
- Decomplexation pathway of Cu(II)-EDTA was analyzed.
- Ligand concentration-dependent decomplexation mechanisms were unveiled.
- Practicability of Mn(II)/PMS process in treating Cu(II) complex wastewater was testified.

GRAPHICAL ABSTRACT

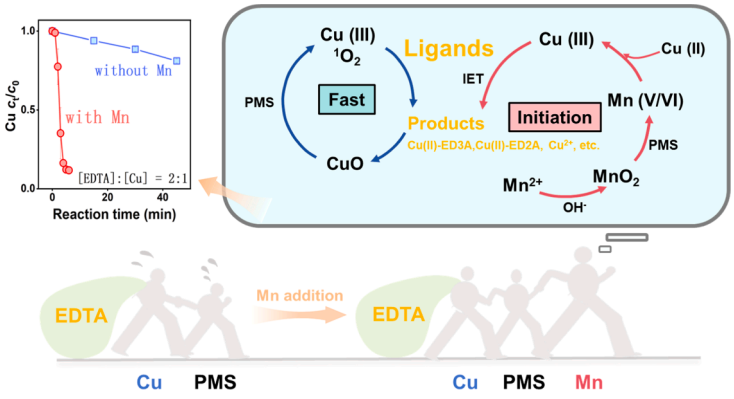

ARTICLE INFO

Keywords:
Cu(II) complexes
Oxidative decomplexation
Ligand excess
Mn(II)/PMS system
Cu-Mn synergism effect

ABSTRACT

The speciation compatibility of Cu-ligand complexes and catalytic oxidation systems fundamentally governs their decomplexation efficiency, exhibiting pronounced ligand concentration dependence. While contemporary methodologies predominantly focus on stoichiometric Cu(II)-ligand complexes, their efficacy in treating wastewater with ligand excess remains technologically contentious. This study demonstrates the Mn(II)/peroxymonosulfate (PMS) process as a robust solution for the elimination of Cu(II)-ligand complexes even in excessive ligand environments. Using Cu(II)-EDTA as the representative complex, 90% decomplexation was achieved within 1 and 5 min at $[EDTA]_0$:[Cu] ratios of 1:1 and 2:1, respectively, surpassing reported

Abbreviations: HM, Heavy metal; SED, Self-enhanced decomplexation; PDS, Peroxydisulfate; EDTA, Ethylenediamine tetraacetic acid; PMS, Peroxymonosulfate; NTA, Nitrilotriacetic acid; RhB, Rhodamine B; EtOH, Ethanol; HA, Humic acid; FFA, Furfuryl alcohol; TBA, Tert-butanol; PP, Sodium pyrophosphate; ED3A, Ethylenediamine triacetic acid; ED2A, Ethylenediamine-*N*,*N*'-diacetic acid; EDMA, *N*-(2-aminoethyl)glycine; EPR, Electron paramagnetic resonance; DMPO, 5,5-dimethyl-1-pyrroline *N*-oxide; TEMP, 2,2,6,6-tetramethylpiperidine; HEDP, Etidronic acid; NCP, Neocuproine.

* Corresponding author at: Guangdong Key Laboratory of Environmental Catalysis and Health Risk Control, Guangdong-Hong Kong-Macao Joint Laboratory for Contaminants Exposure and Health, Institute of Environmental Health and Pollution Control, Guangdong University of Technology, Guangzhou 510006, China.
E-mail address: zxu@gdut.edu.cn (Z. Xu).
[1] These authors contributed equally to this work

https://doi.org/10.1016/j.jhazmat.2026.141833
Received 25 October 2025; Received in revised form 16 March 2026; Accepted 19 March 2026
Available online 20 March 2026

decomplexation approaches such as UV/H_2O_2, UV/peroxydisulfate (PDS), and Co^{2+}/PMS. Mechanistic investigations through oxidation species characterization and product analysis revealed a successive decarboxylation of EDTA by non-radical pathway, i.e., high valence metals and singlet oxygen, enhancing process selectivity while minimizing oxidant consumption ($[PMS]_0$:$[EDTA]_0$ = 30:1). The system exhibits dual mechanistic regimes: (i) instantaneous decomplexation under ligand-deficient conditions via PMS activation by in-situ formed CuO through alkaline precipitation, and (ii) cascade decomplexation for ligand-rich systems involving Mn-Cu synergistic destruction of excessive EDTA prior to CuO-catalyzed degradation of residual ligand. Such synergism is believed to stem from the electron transfer from Cu(II) to Mn(V/VI), forming reactive Cu(III) for decomplexation through intramolecular electron transfer. The Mn(II)/PMS system also exhibited the applicability in treating various Cu(II)-ligand complexes and real wastewater. This work establishes a practical strategy for reliable treatment of industrial wastewater containing non-stoichiometric Cu-ligand complexes.

1. Introduction

Extensive application of copper (Cu) in industrial activities such as electroplating, etching, and alloy production generates substantial amounts of copper-containing wastewater [1–3]. Inadequate treatment and improper disposal practices have led to significant copper discharge into water bodies, with developing countries facing particularly severe challenges due to lax regulations. The potential chronic liver/kidney damages, neurodegenerative disorders and aquatic ecosystems disruption caused by Cu accumulation [4,5] underscores the urgency for advanced remediation strategies to mitigate copper pollution's cascading impacts. Although lots of methods including adsorption, chemical precipitation, ion exchange, zero valent iron, electrodialysis and electroreduction are capable of separating labile Cu from wastewater, a great proportion of Cu(II) in industrial wastewater, e.g., electroplating, electronics manufacturing, metallurgy, and dyeing effluents, exists as recalcitrant Cu(II)-ligand complexes [6,7] that are hardly removed by those processes due to the stabilization effect of ligands [8], which calls for specific processes to effectively treat wastewater containing both Cu(II) and ligands.

Current strategies for Cu(II)-ligand complexes elimination include replacement decomplexation [9], oxidative decomplexation [10] and coordination adsorption [11], among which oxidative decomplexation is widely adopted because of its robust performance against the fluctuation of inflow quality. To date, a spectrum of oxidation techniques have been documented to degrade the ligands to release Cu^{2+} ions for further treatment, such as ozonation [10], piezoelectric oxidation [12], electro-oxidation [13], Fenton-like systems [14] and plasma oxidation [15], where oxidative species with high reactivity readily destroy the complexing groups. In comparison to parent Cu(II)-ligand complexes that are typically inert, their decomplexation intermediates and released Cu^{2+} may exhibit higher activity for catalytic oxidation and thus accelerating the decomplexation by promoting oxidative species formation, which is known as self-enhanced decomplexation (SED) effect [16–20]. It has been reported that SED effect can drastically improve Cu (II)-ligand complex decomplexation by UV/hydrogen peroxide (H_2O_2) [21], UV/peroxydisulfate (PDS) [21], UV/NaClO [22], electro-membrane [23] etc., therefore outcompete those processes without SED effect. For instance, Huang group found the decomplexation intermediates of Cu(II)-ethylenediamine tetraacetate (EDTA) promoted the reactive oxygen species and reactive chlorine species formation, leading to 3.71-fold increased degradation kinetics [22]. Our previous study evidenced the remarkably facilitated activation of PDS and H_2O_2 by Cu(II)-EDTA decomplexation products in UV/PDS and UV/H_2O_2 systems, respectively [21]. These results emphasize the significance of speciation compatibility in decomplexation.

In spite of the diverse decomplexation systems exhibiting SED effect, ideal conditions were employed in these works [14,17–19,21,22,24–27] where stoichiometric ligands were utilized to prepare complexes as model pollutants (Table S1). However, in real wastewater the concentration of ligands frequently surpasses the stoichiometric relationship. Wastewater with high ligands content tend to show distinct decomplexation features in comparison to stoichiometric Cu(II)-ligand complexes because excessive ligands can not only deactivate the catalysts used for oxidative decomplexation but also hinder the SED effect by retarding active Cu(II) species (such as less stable daughter Cu(II)-ligand complexes and Cu^{2+}) formation [14]. As a result, excessive ligands can invalidate decomplexation techniques, even though they have been proven highly efficient under ideal conditions, and it is therefore critical to seek for ligand concentration-insensitive SED systems for highly efficient decomplexation.

Current studies had verified Cu(II)/peroxymonosulfate (PMS) as a highly efficient Fenton-like system for organics abatement [28], outperforming other Cu(II)/oxidant processes, which hints PMS as a proper oxidant to maximize SED effect of Cu(II)-ligand complexes. However, the performance of Cu(II)/PMS system in decomplexing Cu(II)-ligand complexes remains questionable since the strong affinity between Cu (II) and ligands tends to inhibit the formation of Cu(II)-PMS that is proposed as the key oxidative species of Cu(II)/PMS system [28], necessitating alternative methods to activate PMS when excessive ligands present. Recently, PMS activation by complexed Mn(II) was suggested to be a potential decontamination strategy where Mn(II) was oxidized by PMS to form Mn(V) which may subsequently degraded pollutants with considerable efficiency [29]. Inspired by the above findings, we infer Mn(II)/PMS process to be an excessive ligand-resistant method for Cu(II)-ligand complex wastewater remediation: Mn(II) and Cu(II) species may act as the catalysts for decomplexation when the ligands are excessive and insufficient, respectively. Nonetheless, the feasibility and mechanisms of Mn(II)/PMS process in decomplexing Cu (II)-ligand complexes, especially the speciation evolution and Mn-Cu species interaction, are still unclear.

In this work, comprehensive investigations were conducted to study the decomplexation of Cu(II)-EDTA, a typical complex in industrial wastewater, by Mn(II)/PMS process. The primary objectives include: 1. verifying the feasibility of Mn(II)/PMS in decomplexing Cu(II)-ligand complexes, 2. enclosing the influence factors on Cu(II)-EDTA decomplexation, 3. unveiling the decomplexation mechanism of Cu(II)-EDTA, and 4. elucidating the mechanism on the formation of key oxidative species.

2. Experimental

2.1. Chemicals and reagents

All chemicals and reagents were of analytical grade or higher purity and used as received without further purification. Copper sulfate pentahydrate ($CuSO_4 \bullet 5H_2O$), nickel nitrate ($Ni(NO_3)_2$), cobalt nitrate ($Co(NO_3)_2$), manganese sulfate ($MnSO_4$), PMS, EDTA, citrate sodium, Rhodamine B (RhB) and PDS were purchased from Sigma-Aldrich. Ethylenediamine diacetic acid (ED2A), NTA, etidronate, ethanol (EtOH), humic acid (HA), sodium hydroxide (NaOH), sodium chloride (NaCl), sodium citrate, furfuryl alcohol (FFA), sodium nitrate ($NaNO_3$), tert-butanol (TBA), sodium sulfate (Na_2SO_4), barium chloride ($BaCl_2$), sodium periodate ($NaIO_4$), neocuproine (NCP) and potassium permanganate ($KMnO_4$) were supported by Aladdin. Sodium pyrophosphate (PP) and etidronic acid (HEDP) were supplied by Macklin. $Mn(OH)_2$

powder was bought from Jiuno biotechnology Co., LTD. Ethylenediamine monoacetic acid (EDMA) was bought from Tokyo Chemical Industry (TCI). H_2O_2, chloform ($CHCl_3$), were obtained from Guangzhou Chemical Reagent Factory. 5,5-dimethyl-1-pyrroline N-oxide (DMPO) and 2,2,6,6-tetramethylpiperidine (TEMP) were acquired from J&K chemical.

2.2. Decomplexation experiment

In a typical process, decomplexation of Cu(II)-EDTA by Mn(II)/PMS process was conducted as the following procedure: 8.75 mM PMS was added to simulated wastewater containing 0.15 mM Cu^{2+} and 0.3 mM EDTA. Then 0.06 mM $MnSO_4$ was dosed to initiate the decomplexation after adjusting solution pH to 9.5 by NaOH. Suspension samples were collected at preset time intervals. The sampled suspension was immediately injected into 0.2 M sodium sulfite solution to terminate the decomplexation. Precipitate sampling was carried out by vacuum-filtrating the suspension and then collecting the air-dried filter cake. All samples were stored at 4 ℃ before further analysis.

Decomplexation of complexes was determined based on the removal of Cu. In brief, suspension was filtrated through a 0.22 μm diameter filter to remove the precipitates generated from the spontaneous alkaline-precipitation of decomplexation-released Cu^{2+}. Next, the filtrate was acidified by 10% H_2SO_4 and concentration of Cu was measured through an atomic absorption spectrophotometer (AAS, Shimadzu AA-7800), representing the concentration of non-decomplexed Cu. When the decomplexation was executed under acidic and neutral conditions, pH of the suspension was post-adjusted to 9.5 by NaOH to transform decomplexation-released labile Cu to insoluble precipitates before the filtration. To assess the reusability of the precipitates generated during the decomplexation, solids collected at the tenth min of decomplexation was used, instead of Mn^{2+}, to initiate the treatment of the subsequent batch of Cu(II)-EDTA wastewater. The stability of the precipitate was evaluated by assessing the efficiency of EDTA degradation over consecutive multiple batches.

2.3. Contaminant analysis

Cu(II)-EDTA and its decomplexation intermediates were determined by a high-performance liquid chromatography-mass spectrometer (HPLC-MS, Agilent 1290–6545) equipped with a C18 column (4.6*100 mm 5-Micron) and the detection conditions were identical to previous study [22]. RhB was quantified by an UV–vis spectrophotometer at a wavelength of 554 nm [30].

2.4. Quenching experiment

Quenching experiments were conducted using TBA, EtOH, $CHCl_3$ and FFA as the scavengers for various oxidative species. The procedure is similar to decomplexation experiments but certain scavenger was added before the addition of PMS and Mn(II). The influence of each scavenger was assessed according to the duration of induction stage and kinetics of fast decomplexation stage based on Cu removal.

2.5. Characterization

Solid sample characterization: Transmission electron microscopy (TEM) were applied to observe the morphology. The crystalline properties were probed by X-ray diffraction (XRD) and high-resolution TEM. The chemical microenvironment was detected using X-ray photoelectron spectroscopy (XPS) and Raman spectroscopy, and elemental distribution was obtained through XPS.

Liquid sample characterization: The valence stage of Mn and Cu were analyzed by Raman spectroscopy and UV–vis spectroscopy. Cu(I) and Cu (III) were determined by means of neocuproine [31] and periodate [25] methods, respectively. Mn(III) was measured by UV–vis spectroscopy at 258 nm with the stabilization of PP [32]. The contribution of Mn(V/VI) was investigated by Ba^{2+} through the precipitation of $BaMnO_4$ [33]. Mn (VII) was detected by UV–vis spectroscopy at 525 nm [34]. Cu(III) solution was prepared according to the reported method [25]. Electron paramagnetic resonance (EPR) was employed to probe hydroxyl radicals (HO•), sulfate radicals ($SO_4^{\bullet-}$), superoxide anion radicals ($O_2^{\bullet-}$) and singlet oxygen ($^1O_2$). DMPO was used to capture HO•, $SO_4^{\bullet-}$ and $O_2^{\bullet-}$, while $^1O_2$ was detected by TEMP.

3. Results and discussion

3.1. Decomplexation efficiency

The decomplexation efficiency of stoichiometric Cu(II)-EDTA was systematically evaluated using three peroxides, including H_2O_2, PDS, and PMS, across varying pH conditions to elucidate the catalytic role of Cu species in peroxide activation (Fig. 1). Under acidic and neutral conditions (pH 3.0 and 6.8), all peroxides exhibited limited efficacy, achieving $<$ 15% Cu(II)-EDTA decomplexation within 20 min. In contrast, alkaline conditions (pH 9.5) significantly enhanced the reaction kinetics when PMS was employed, achieving complete decomplexation in 60 s, consistent with the catalytic activity of non-complexed Cu(II) toward peroxide activation as quantified by RhB degradation dynamics (Fig. S1). This pH-dependent behavior confirms that the PMS/alkaline system optimally exploits the auto-catalytic effect for Cu(II)-EDTA decomplexation.

Notably, the process efficiency exhibited strong ligand concentration dependence. While stoichiometric Cu(II)-EDTA ($[EDTA]_0$:[Cu] = 1:1) demonstrated effective decomplexation, systems with excessive EDTA ($[EDTA]_0$:[Cu] = 2:1) showed negligible decomplexation within 45 min (Fig. S2), indicating remarkable suppression of Cu-mediated catalysis. This inhibitory effect was further corroborated by the limited performance of UV/H_2O_2, UV/PDS, Co^{2+}/PMS and Fenton systems under ligand excess conditions (Fig. 2a), despite their reported superiority in decomplexing stoichiometric Cu(II)-EDTA, which is attributed to EDTA-induced passivation. Theoretically, the chelating capacity of EDTA not only poisons Cu centers but also extends to other transition metal ions (e.g., Fe, Co) and heterogeneous catalysts, thereby compromising conventional advanced oxidation processes. These findings highlight strategies to simultaneously address ligand interference while utilizing endogenous Cu for catalytic cycles.

Inspired by the reported high efficiency of PMS activation by Mn(II) complexed with coexisted ligands [22], we systematically investigated the Mn(II)/PMS system for decomplexing Cu(II)-EDTA at different stoichiometric ratios ($[EDTA]_0$:[Cu] = 1:1–2:1). The EDTA concentration- and Mn(II) dose-responses confirmed the feasibility of Mn(II)/PMS system (Fig. 2a-c), revealing a remarkable catalytic effect where trace Mn(II) (as low as 0.02 mM) triggered rapid decomplexation following a two-phase kinetic profile: an initial induction stage and subsequent rapid decomplexation stage. Time required to reach 90% decomplexation is 5 min, surpassing other processes even though excessive EDTA was used in this study [14,18]. The temporal evolution of total organic carbon (TOC) during the reaction was monitored (Fig. S3). Surprisingly, TOC exhibited a rapid decline during the induction stage, with half of the TOC removed within two minutes. In contrast, the rapid decomplexation stage only marginally reduced TOC, with 43% TOC retention even after complete Cu release. This suggests that the rapid decomplexation stage likely transformed strongly complexing ligands into weakly complexing small organic molecules rather than mineralization.

PMS dosage positively correlates with decomplexation efficiency but inversely relates to induction period (Fig. S4). Notably, optimal performance occurred at $[oxidant]_0$:$[EDTA]_0$ = 30:1, alleviating the oxidant consumption compared to literature values (50:1, 150:1, and 50:1 for UV/PDS, UV/H_2O_2, and Co^{2+}/PMS, respectively) [14,18]. Decomplexation curves at various pHs demonstrate Mn(II)/PMS an

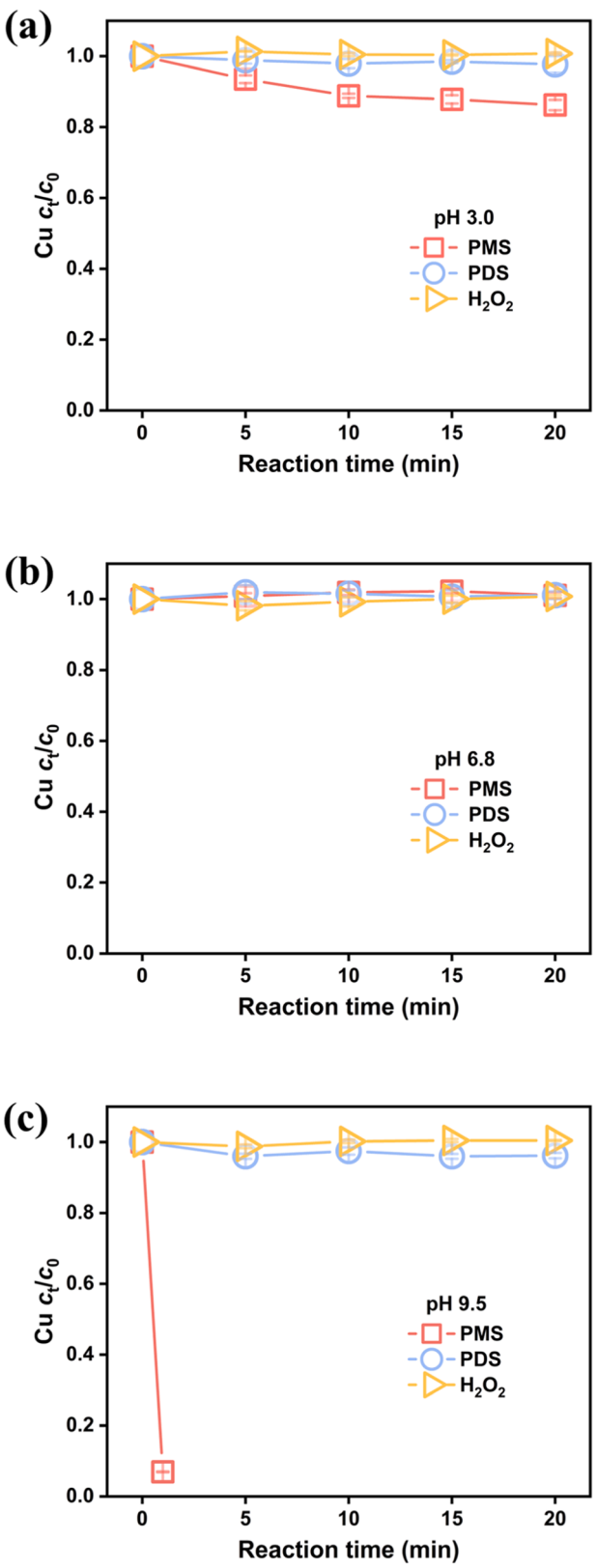

Fig. 1. Decomplexation of stoichiometric Cu(II)-EDTA by oxidant alone at various pHs, (a) pH 3.0 (b) pH 6.8 (c) pH 9.5 (conditions: [Cu] = $[EDTA]_0$ = 0.15 mM, $[oxidant]_0$ = 8.75 mM, T = 298 K. Post-precipitation (pH 9.5) was used to remove released Cu when decomplexation was conducted at pHs 3.0 and 6.8).

alkaline-favored process (Fig. S5), whereas no obvious decomplexation happened under acidic and neutral conditions, which may associate with two factors: (i) catalytically active Cu precipitates are exclusively formed under alkaline conditions (Fig. S6) and (ii) the deprotonated SO_5^{2-} showed higher activation propensity compared to its protonated form HSO_5^- (pKa_2 = 9.4) [35,36]. The system exhibited exceptional robustness against most common background anions (Fig. S7). The Cl^--insensitive decomplexation kinetics contrasts with radical-dominated advanced oxidation processes, suggesting non-radical species dominated pathways. While the negative influence of HA may associate with the competitive consumption of oxidative species because of its reducing and electron-rich structures (Fig. S8). In addition, the Mn(II)/PMS process effectively treated diverse Cu (II)-ligand complexes (NTA, citrate, HEDP), accomplishing almost decomplexation in 3 min, 4 min and 15 min, respectively, under identical operational conditions (Fig. 2d). In contrast, the absence of Mn addition resulted in a 23 min requirement for 90% decomplexation of Cu(II)-NTA, whereas less than 10% of Cu was released from Cu (II)-citrate and Cu(II)-HEDP within 60 min (Fig. S9), demonstrating the broad applicability of the Mn(II)/PMS system in decomplexing Cu (II) complexes.

3.2. Decomplexation pathway

The speciation analysis of Cu(II)-EDTA and its degradation intermediates was conducted to elucidate the decomplexation progress. The sequential detection of Cu(II)-ED3A and Cu(II)-ED2A intermediates (Fig. 3), accompanied by the ambiguous characteristic signatures of Cu (II)-NTA and Cu(II)-IMDA, unequivocally demonstrates a stepwise decarboxylation-driven decomplexation pathway for Cu(II)-EDTA [29]. Detailed examination of ligand evolution kinetics during the induction stage reveals two distinct regimes, showing minimal degradation within the initial 60 s, followed by an abrupt acceleration of decarboxylation in the following minutes (Fig. 3b). The stabilization capacities of various ligands were quantitatively assessed through alkaline precipitation experiments (Fig. S10). The negligible precipitation of Cu(II)-EDTA and moderate precipitation of Cu(II)-ED2A and Cu(II)-EDMA substantiate the critical requirement for EDTA transformation into ED2A or more oxidized species for Cu hydrolysis, and advanced removal of Cu was only achieved when ligands were almost destroyed.

3.3. Oxidative species

The mechanistic investigation of Cu(II)-EDTA decomplexation was systematically conducted through comprehensive analysis of oxidative species. EPR spectroscopy reveals weak HO• signals and negligible signals for $O_2^{\bullet-}$, while $^1O_2$ was clearly identified as participating species (Fig. 4a and b). Quantitative assessment of oxidative species contributions was achieved through quenching experiments employing TBA, EtOH, chloroform, and FFA as scavengers for different oxidative species [37,38]. The quenchers were added before the decomplexation and during the rapid decomplexation stage to study their influence on the induction time and decomplexation kinetics, respectively. In accordance with EPR results, the presence of HO• scavenger TBA inhibited the decomplexation to some extent, indicating the contribution of HO•, whereas the negligible inhibition effects observed with chloroform treatment excluded $O_2^{\bullet-}$ as primary oxidative species. The decomplexation was almost inhibited when EtOH and FFA were added before the decomplexation (Fig. 4c). Considering the absent $SO_4^{\bullet-}$ signal and weak signal of HO•, it is concluded that high-valent metal species serve as important oxidants during the induction stage, which is consistent with the detected Cu(III) (Fig. S11) and the quenching of high-valent metal species by EtOH (Fig. S12) [22,39]. However, the introduction of EtOH and FFA during the rapid decomplexation stage did not completely prevent the decomplexation (Fig. 4d), causing 64% and 85% deceleration, respectively, demonstrating distinct oxidative species in

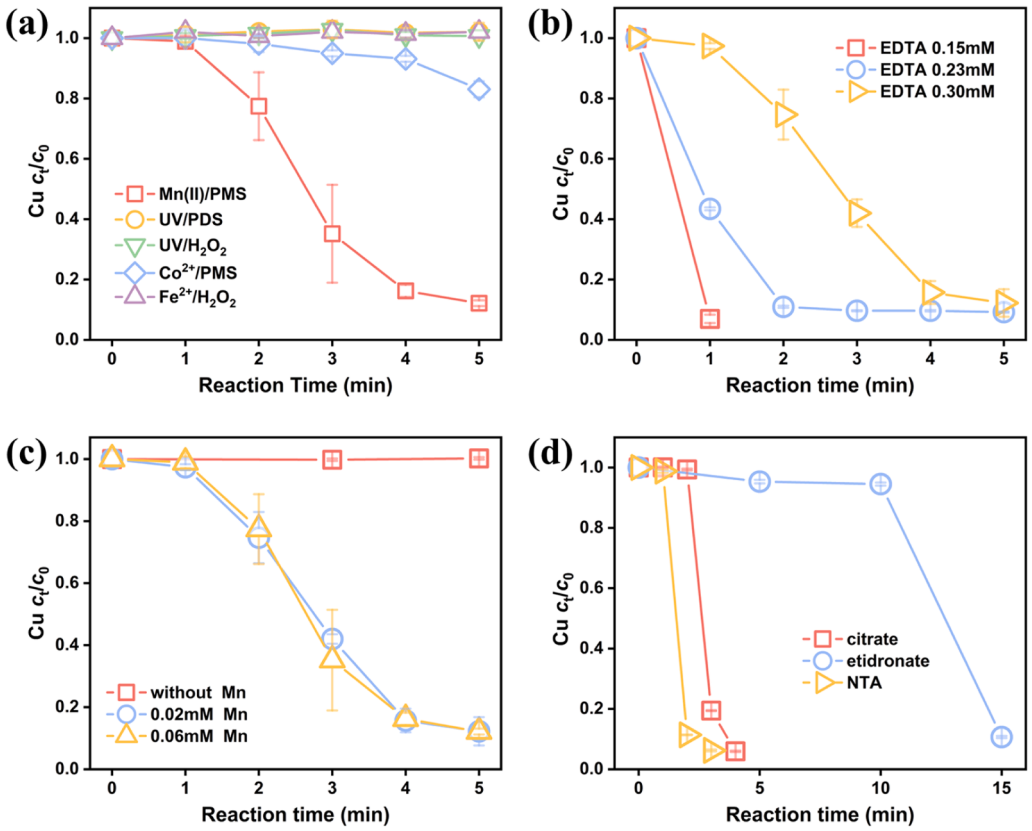

Fig. 2. Decomplexation of Cu(II)-ligand complexes with excessive ligands, (a) decomplexation of Cu(II)-EDTA by Mn(II)/PMS, UV/PDS, UV/H_2O_2, Co^{2+}/PMS and Fe^{2+}/H_2O_2 processes, (b) and (c) influence of EDTA and Mn concentrations on Cu(II)-EDTA decomplexation, (d) decomplexing various Cu(II)-ligand complexes by Mn(II)/PMS process (all processes were conducted at optimal conditions: [Cu] = 0.15 mM, $[ligand]_0$ = 0.30 mM, $[oxidant]_0$ = 8.75 mM, T = 298 K, pHs were maintained at 9.5 and 3.0 in Mn(II)/PMS and other processes, respectively).

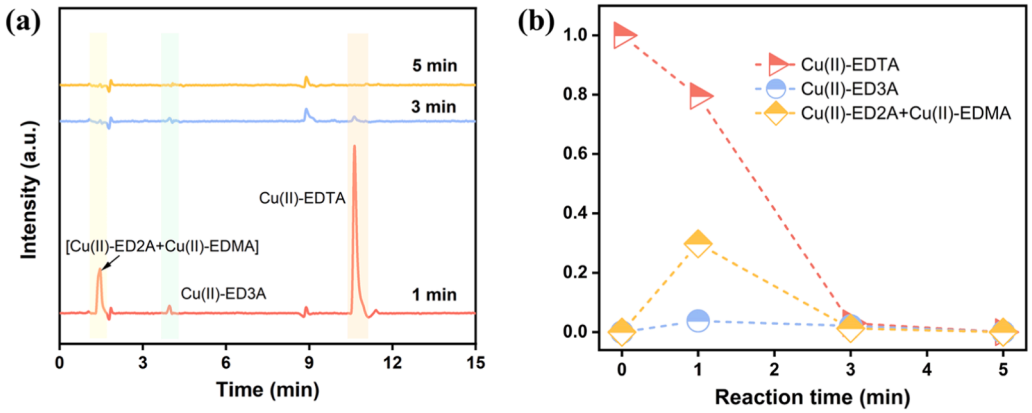

Fig. 3. (a) HPLC results of solutions at different reaction time, (b) concentrations of Cu(II)-EDTA and decomplexation products.

each stage. The most pronounced inhibition by FFA stems from its dual reactivity toward both reactive oxygen species and high-valence metal species, thereby confirming oxidative reactions rather than replacement reactions as the governing decomplexation pathway. The much stronger inhibitory effect of ethanol than TBA, together with the ambiguous signal of $SO_4^{\bullet-}$ (Fig. S13), indicates that high-valent metal species remain important during the rapid decomplexation stage. Comparing the quenching effects of EtOH and FFA in the two stages, it is suggested that the non-radical oxidative species $^1O_2$ plays a minor role during the induction stage but contributes to the rapid decomplexation stage.

3.4. Role of Mn and Cu species

Investigations of the induction stage reveal the catalytic behaviors of copper and manganese species. Speciation analysis demonstrates that in this stage copper predominantly existed as dissolved state complexed by strong ligands, which exhibits limited PMS activation capability (Fig. S14). This observation initially suggests manganese species as the principal catalytic drivers during early reaction stages. However, systematic evaluation of Mn(II)/PMS and Mn(II)/EDTA/PMS systems, employing RhB degradation as a probe reaction, yields opposite conclusions (Fig. 5a). The observed degradation kinetics shows no significant enhancement compared to control systems lacking manganese (k_{obs}

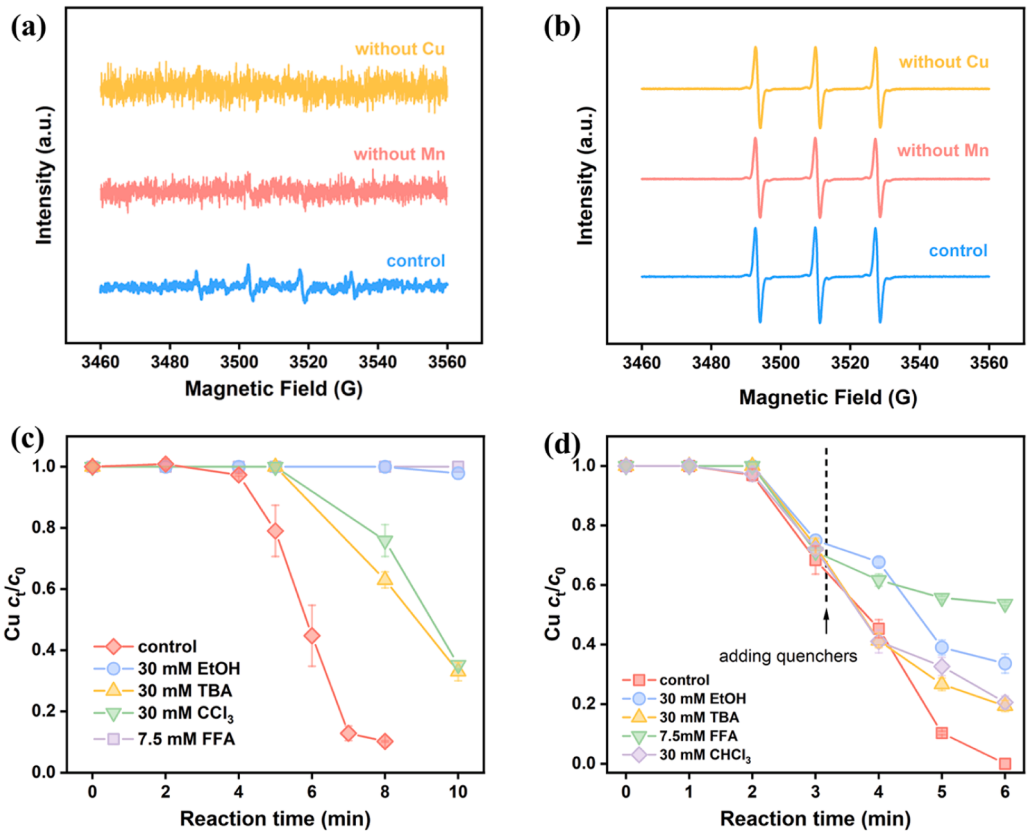

Fig. 4. Identifying the importance of oxidative species for Cu(II)-EDTA decomplexation, (a) and (b) EPR analysis using DMPO and TEMP as the capturers for samples collected during the induction phase, (c) and (d) quenching experiments where quenchers were added before the decomplexation and during the rapid decomplexation stage ([Cu] = 0.075 mM, $[EDTA]_0$ = 0.15 mM, $[oxidant]_0$ = 5 mM, pH = 9.5, T = 298 K).

ranged from 0.083 to 0.095 min^{-1} in all systems). To assess whether this phenomenon arises from selective oxidation of EDTA over RhB by Mn-induced reactive species, we compared the degradation of EDTA in both EDTA/PMS and Mn(II)/EDTA/PMS systems. The results revealed comparable EDTA removal efficiencies between the two systems (Fig. S15), suggesting that the observed effect is not due to selective oxidation of EDTA, thereby underscoring copper's indispensable role. Combining with the minimal RhB removal in Cu(II)/EDTA/PMS systems (Fig. 5a), it is suggested that neither copper nor manganese species alone can effectively activate PMS during the induction phase. The drastic improvement in degradation efficiency observed in the Mn(II)/Cu(II)/EDTA/PMS system (k_{obs} = 0.621 min^{-1}) provides sound evidence for a synergistic catalytic mechanism between manganese and copper.

Contrary to copper's homogeneous distribution, manganese exhibits dual-phase characteristics during the induction stage, with both dissolved and solid-phase species. The contributions of dissolved and solid species were distinguished by filtration-decomplexation experiments where solid species was removed through vacuum filtration every 60 s (Fig. 5b). The remarkably inhibitory effect necessitates the involvement of manganese precipitates in the decomplexation process. Subsequent experiments employing pre-formed manganese precipitates (collected from Mn(II)/EDTA/PMS systems) achieved 78% copper removal within 7 min, with an induction period of 2 min (Fig. S16), conclusively demonstrating the importance of solid-phase manganese species. Comprehensive characterizations of these precipitates identify them as MnO_2 (Fig. 5c and d), with high-resolution imaging confirming the presence of MnO_2 nanocrystals. The absence of other manganese oxidation states in XPS spectra (Mn $2p_{3/2}$ binding energy ~ 641.8 eV) validates the phase purity of these catalytically active precipitates (Fig. S17).

The distinct oxidative efficiencies observed across various copper- and manganese-based systems, combined with identified reactive species, collectively suggest the interaction between copper and manganese species. This inference is also supported by metal-specific decomplexation behaviors: the Mn(II)/PMS system exhibited effective decomplexation for Cu(II)-EDTA but showed poor efficacy for Ni(II)-EDTA and Co(II)-EDTA mitigation (Fig. S18). To probe this interaction mechanism, we systematically monitored valence state transitions of both metals during the reaction process.

Copper may exist as stable Cu(II) and unstable Cu(I) and Cu(III) in water, among which Cu(III) have been reported to be an effective oxidant for EDTA degradation [29], consistent with our results that the prepared Cu(III) was completely consumed by EDTA in 5 min (Fig. S19). Notwithstanding the relatively weak signals of Cu(III) species detected by UV–vis spectroscopy and in-situ Raman analysis in induction stage (Fig. 4d and S20), prior investigations have established the occurrence of rapid intramolecular electron transfer from organic ligands to Cu(III) centers [17]. This dynamic factor results in low steady-state concentrations of Cu(III) due to its instantaneous reduction to Cu(II) by excessive EDTA. Significantly, this ligand-to-metal charge transfer mechanism builds a selective oxidation pathway that minimizes oxidant consumption [17,28], consistent with the lower dosage required to achieve complete decomplexation in comparison to radical-dominated processes where non-selective $SO_4^{\bullet-}$ and HO• tend to react indiscriminately with both target complexes and ubiquitous matrix components (e.g., Cl^- and NOM) and self-quenching. Therefore, with the remarkable reactivity and selectivity, the formation of Cu(III) is assumed to be critical for the decomplexation. The absence of Cu(I) throughout the decomplexation demonstrates the generation of Cu(III) through one-electron transfer of Cu(II) but not two-electron transfer of Cu(I) (Fig. S21), implying the oxidation of Cu(II) by oxidative Mn species.

Oxidative Mn(III) was first monitored based on the characteristic

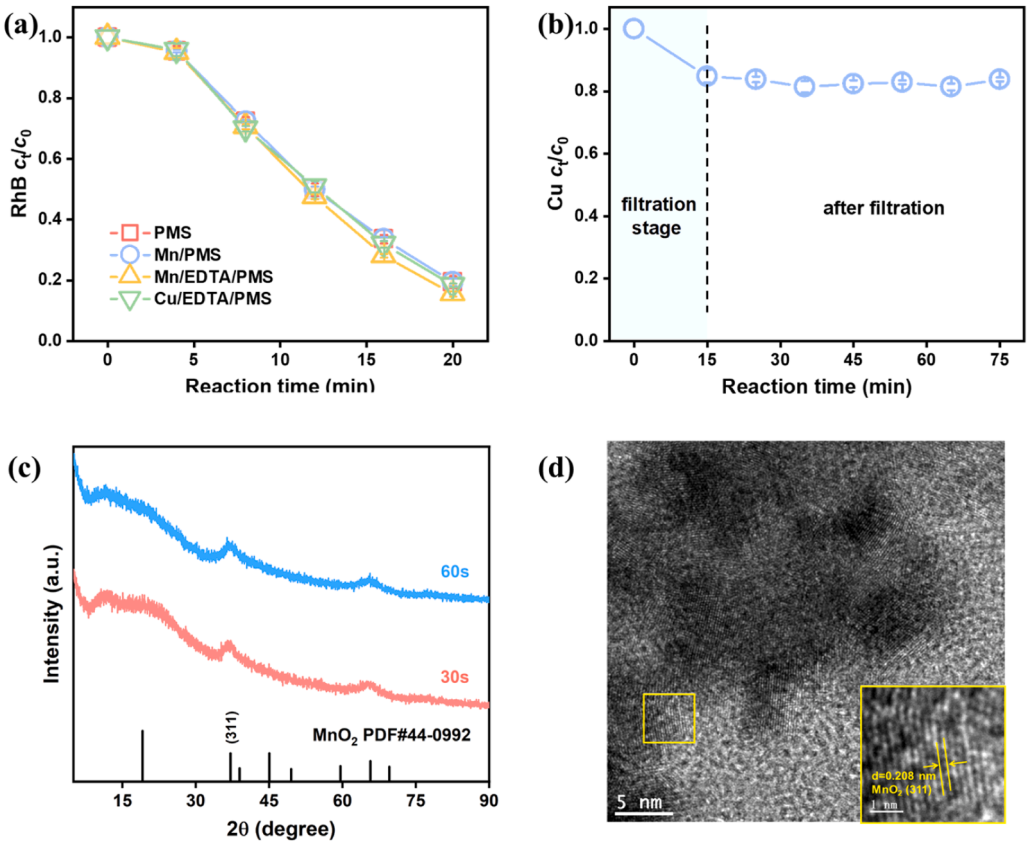

Fig. 5. (a) Decolorization of RhB by PMS, Mn(II)/PMS, Mn(II)/EDTA/PMS and Cu(II)/EDTA/PMS systems ([Cu] = 0.15 mM, [Mn] = 0.15 mM, $[EDTA]_0$ = 0.3 mM, $[PMS]_0$ = 8.75 mM, pH = 9.5, T = 298 K), (b) Cu(II)-EDTA decomplexation in a filtration-decomplexation experiment ([Cu] = 0.15 mM, $[EDTA]_0$ = 0.3 mM, $[PMS]_0$ = 8.75 mM, [Mn] = 0.06 mM, pH = 9.5, T = 298 K, filtration was conducted every 60 s in the first 15 min), (c) XRD patterns of the precipitates in the induction stage, (d) typical TEM image of the precipitate in the induction stage.

absorption of Mn(III)-PP and Mn(III)-EDTA complexes (Fig. S22a). The negligible characteristic peak after adding Mn^{2+} reflects the insignificant role of Mn(III), consistent with the limited decomplexation of Cu(II)-EDTA by ex-situ prepared Mn(III) solution by mixing $MnSO_4$ and $KMnO_4$ (Fig. S22b) [40]. The negligible decomplexation by MnO_2 alone also rules out the oxidation of Cu(II) by Mn(IV). Experiments with increased concentrations were conducted to probe high valent Mn species given their low steady concentrations. Notably, typical absorption spectrum of $KMnO_4$ emerged when solutions simultaneously contained Mn^{2+} and PMS (Fig. S23a), which agrees with the susceptibility of MnO_2 under alkaline conditions [41]. Using $KMnO_4$ instead of Mn^{2+} and PMS, however, did not promote the decomplexation (Fig. S23b), thus excluding active species generation through a permanganate-mediated pathway. Considering permanganate formation from Mn(II/IV) usually involves high-valence Mn intermediates (Mn(V/VI)) that enable effective organics degradation, attempt was made to probe the formation of Mn(V/VI) by PMSO [29,33] and Ba^{2+} methods [25,31]. However, $PMSO_2$ was detected both in the presence and absence of manganese, attributed to the reaction between PMSO and $^1O_2$ produced through the decomposition of PMS under experimental conditions. As for Ba^{2+} method, an accelerated decomplexation was observed after Ba^{2+} addition (Fig. S24), demonstrating unexpected side-reactions to confuse the results, which may associate with the increased ionic strength and promoted PMS activation by alkaline-earth metal precipitates [26,42]. Despite the experimental challenges in probing high-valent manganese species in complex aqueous environments, we posit its pivotal role in decomplexation because of the essentiality of manganese and the limited efficacy of manganese in other oxidation states in our system. It has been documented that Mn(V/VI) can act as both single-electron and two-electron oxidant [34], we therefore deduce the one-electron oxidation of Cu(II) by Mn(V/VI). Given that no reduced Cu species (i.e., Cu(I)) was detected during the reaction, Cu(II) is not involved in Mn oxidation, and the formation of Mn(V/VI) is driven solely by PMS. Nevertheless, negligible ligand degradation was observed in the absence of Cu, and Cu(III) was only detected upon Mn addition, indicating that Mn(V/VI) is less effective than Cu(III) for ligand degradation, and that Cu(II)-mediated processes significantly accelerate the decomplexation.

The reaction progression was marked by distinct chromatic transitions, with the solution evolving from brown during the induction phase to black in the rapid decomplexation stage. These visual changes correlate with the sequential formation of MnO_2 and CuO nanoparticles, as conclusively verified by XRD crystallography and high-resolution TEM imaging (Fig. 6a and b). The observed acceleration of decomplexation dynamics during the rapid phase strongly implicates the catalytic activity of in-situ generated CuO precipitates. This interpretation aligns with the exceptional oxidative capacity of CuO/PMS systems and the extremely fast decomplexation of Cu(II)-ligand complexes where the ligands cannot completely prevent the alkaline-precipitation of Cu(II) (Fig. 6c and S10). Furthermore, the characteristic pH decrease associated with CuO/PMS chemistry was confirmed upon initiation of the rapid decomplexation phase, providing additional evidence for the proposed catalytic mechanism.

Extensive research has demonstrated that the catalytic performance of transition metal precipitates can be engineered through ligand coordination and secondary metal incorporation, which effectively modulates their electronic configurations and surface energetics. To elucidate the roles of Mn(II) and EDTA in modifying CuO precipitate catalysis, we systematically evaluated the precipitates formed in Cu(II)/PMS, Cu(II)/Mn(II)/PMS, Cu(II)-EDTA/PMS, and Cu(II)/Mn(II)/EDTA/PMS systems. Kinetic analyses reflect comparable RhB degradation profiles for all

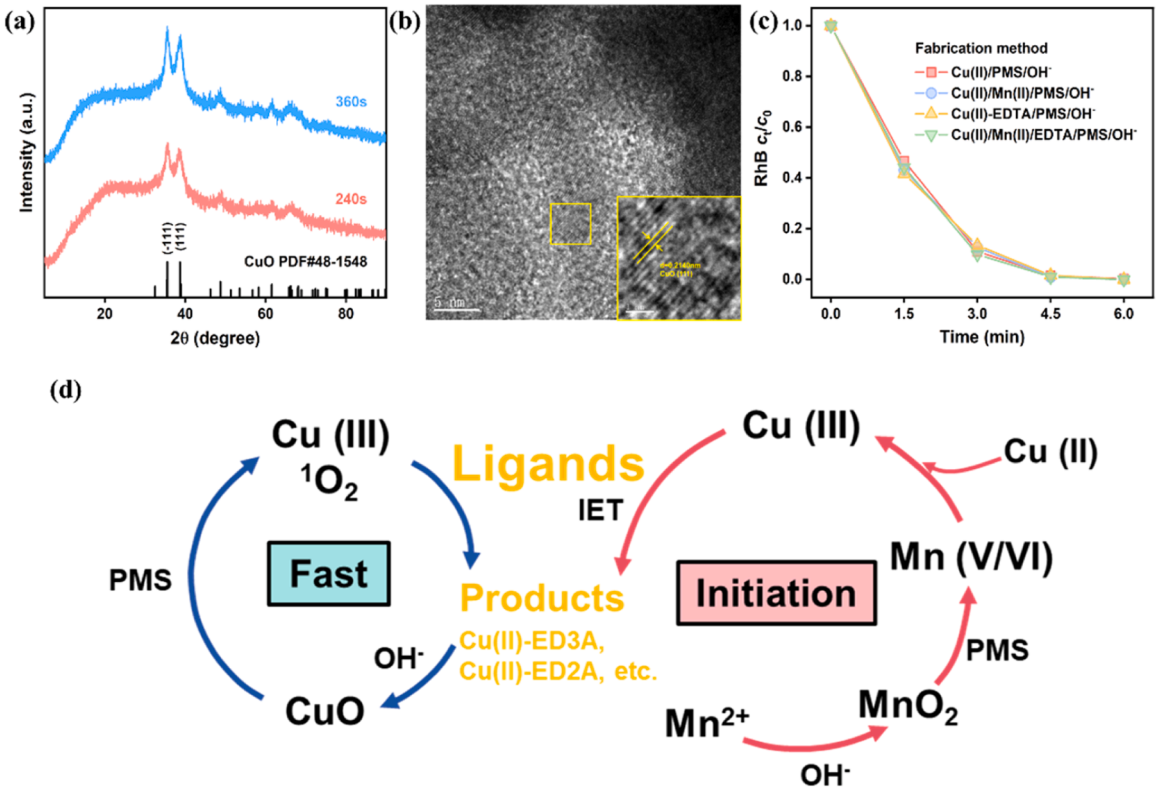

Fig. 6. (a) XRD patterns of the precipitates in the rapid decomplexation stage, (b) typical TEM image of the precipitates in the rapid decomplexation stage, (c) activating PMS by various precipitates to degrade RhB ([precipitate] = 30 mg/L, [RhB] = 0.1 mM, [PMS] = 5 mM), (d) schematic diagram of Cu(II)-EDTA decomplexation by Mn(II)/PMS process.

samples (Fig. 6c), indicating conserved PMS activation regardless of the preparation conditions. These collective findings suggest that the intrinsic catalytic activity of crystalline CuO dominates the oxidative processes in the rapid decomplexation stage, with Mn(II) and EDTA exerting negligible influence on its catalytic behaviors, even though Mn species acts a critical role in the induction stage. Therefore, the high-valent metal species that plays a major role in the rapid decomplexation stage is Cu(III) rather than high-valent Mn. The adsorptive removal of Cu(II)-EDTA by Mn- and Cu-precipitates is also excluded given its unchanged concentration during the adsorption experiments (Fig. S25).

Although MnO_2 was identified as the sole Mn phase in the final precipitate, other Mn species may also participate in the decomplexation, especially in the induction stage. Since $Mn(OH)_2$ is usually recognized as an early product of Mn^{2+} hydrolysis, commercial Mn $(OH)_2$ was used to evaluate its capacity in decomplexing Cu(II)-EDTA. The fast decomplexation after $Mn(OH)_2$ addition demonstrates the potential contributions of $Mn(OH)_2$ (Fig. S26). To unveil whether $Mn(OH)_2$ was produced during Mn^{2+} hydrolysis, XRD and high-resolution TEM were employed to identify the crystalline structure. XRD patterns indicate that, regardless of the presence of PMS, the short-term hydrolysis products of manganese ions exhibit no distinct crystalline signals, suggesting weak crystallinity of the precipitates during the induction stage (Fig. S27). Although the long-range structure is disordered, TEM images reveal the presence of many nanocrystals within the precipitates. In the absence of PMS, these crystals consist of $Mn(OH)_2$ and MnO_2 (Fig. S28), while only MnO_2 was detected in the presence of PMS (Fig. S29), likely due to the oxidation of $Mn(OH)_2$ by PMS. It is therefore inferred that during the decomplexation process, the content of MnO_2 exceeds that of $Mn(OH)_2$. Moreover, compared to Mn(II) in $Mn(OH)_2$, Mn(IV) in MnO_2 is more favorable for further transformation into higher-valent manganese species (Mn(V/VI)) to trigger the decomplexation. Consequently, although the role of amorphous Mn structure and initially formed Mn $(OH)_2$ cannot be excluded, MnO_2 is believed to be the key catalytic species.

Based on above analyses, the comprehensive reaction mechanism for Cu(II)-EDTA decomplexation in Mn(II)/PMS systems is schematically illustrated in Fig. 6d. Under Cu(II)-excess conditions, non-complexed Cu^{2+} ions undergo immediate alkaline precipitation to form highly active CuO nanoparticles. These nanostructures catalyze PMS activation through transient Cu(III) and singlet oxygen ($^1O_2$) generation, which subsequently attack parent and daughter ligands. The liberated Cu^{2+} from ligand oxidation further transforms to CuO to promote the decomplexation, thus establishing a beneficent loop that exponentially accelerates decomplexation kinetics. Conversely, in EDTA-dominant systems ([Cu]:$[EDTA]_0$ < 1), the decomplexation was markedly inhibited due to the coordination stabilization. Here, Mn(II) plays a pivotal role through its alkaline precipitation into MnO_2 and then to high valent species, which mediates the oxidation of Cu(II) to Cu(III). Subsequent intramolecular electron transfer from EDTA to Cu(III) initiate ligand destabilization via sequential decarboxylation, producing ED3A, ED2A and EDMA as intermediates before complete mineralization. The progressive ligand degradation by high valence metals liberates copper ions that nucleate into fresh CuO nanoparticles, and the decomplexation enters CuO-driven rapid decomplexation stage afterward.

The distinct decomplexation behaviors observed in the two stages prompted a systematic investigation into their reaction characteristics. As illustrated in Fig. S30, although Mn addition significantly enhanced the oxidative capacity of the induction stage, the accelerated degradation of RhB under ligand-deficient conditions suggests that the yield of oxidative species remained markedly lower than that in the rapid decomplexation stage. To further evaluate PMS utilization efficiency in each stage, experiments were conducted under both ligand-excess and ligand-deficient conditions with low PMS dosage. Results revealed that, upon complete PMS consumption, the TOC removal efficiency under

ligand-deficient conditions was approximately 2.1-fold higher than that under ligand-excess conditions (Table S2), highlighting the superior PMS utilization efficiency driven by the Mn-Cu synergistic effect during the induction stage.

3.5. Applicability of Mn(II)/PMS system

The solids collected after Cu(II)-EDTA decomplexation was used instead of $MnSO_4$ to treat the Cu(II)-EDTA wastewater. Fig. S31 demonstrates an immediate decomplexation after solid addition, confirming the reusability of the solids. In comparison to Mn(II)/PMS process, lower decomplexation (~75% Cu released) was achieved by the precipitate/PMS system at the same $[PMS]_0$:$[EDTA]_0$ ratio, which is associated with the higher PMS utilization efficiency in the Mn-Cu system. Furthermore, the stability of the precipitates was evaluated through a consecutive 3-cycle degradation experiment. To avoid the interference from newly generated copper precipitates during Cu(II)-EDTA decomplexation, EDTA was used as the model pollutant. The results show that the degradation rate of EDTA decreased with increasing treatment cycles (Fig. S32), with EDTA removal efficiencies of 100%, 88%, and 69% obtained from the first to the third cycle, respectively. This indicates that the precipitate retains a certain level of catalytic activity under repeated batch operations. The decline in EDTA removal over cycles may be attributed to partial dissolution of the precipitates by EDTA (and its degradation products) and precipitate aging.

The applicability of Mn(II)/PMS system in treating real wastewater was further testified by decomplexing an anodizing wastewater from a metal processing plant (Dongguan, China). The sampled wastewater had been pre-treated by Fe(III) coagulation, which typically leads to ligand-excess environments due to its capacity in removing Cu but not the ligands [9,43], and the typical EDTA to Cu ratios have been experimentally examined (Table S3). Cu content before the decomplexation was measured to be 5.1 mg/L and pH is 9.23 (composition of the wastewater is listed in Table S4). Alkaline-precipitation treatment led to negligible removal of Cu, reflecting Cu presented as stable complexes in the wastewater. While decomplexation by PMS alone could be ignored, co-addition of Mn^{2+} and PMS caused more than 90% decomplexation in 30 min (Fig. 7), meeting the industrial wastewater discharge standard of China (0.5 mg/L), proving the superiority of the Mn(II)/PMS process in treating real Cu(II) complex wastewater.

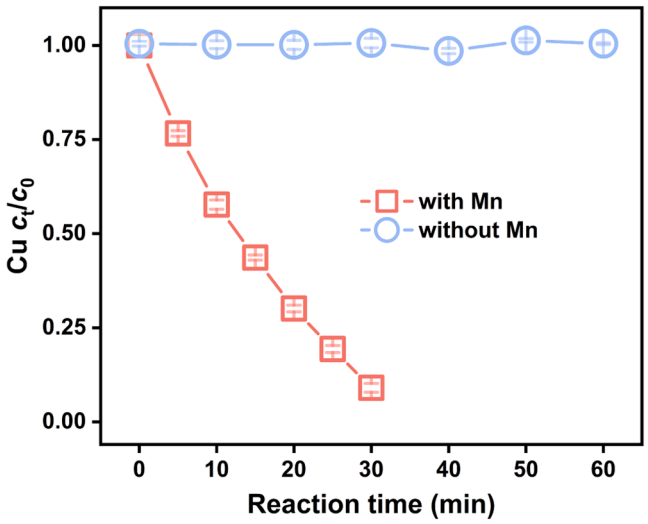

Fig. 7. Decomplexation of a real anodizing wastewater containing complexed Cu ([Cu] = 5.1 mg/L, $[PMS]_0$ = 3.5 mM, [Mn] = 0.06 mM, pH = 9.5, T = 298 K).

4. Conclusions

This study elucidates the Mn(II)/PMS process as an efficacious and ligand concentration-insensitive advanced oxidation strategy for the remediation of copper-ligand complexes. Employing Cu(II)-EDTA as a model contaminant, quantitative decomplexation of Cu was accomplished within short durations of 1 min and 5 min for $[Cu(II)]$:$[EDTA]_0$ molar ratios of 1:1 and 2:1, respectively, under optimized reaction parameters (60 μM Mn(II) and 8.75 mM PMS, $[PMS]_0$:$[EDTA]_0$ = 30:1). The system demonstrated exceptional resilience against ubiquitous coexisting anions while maintaining superior decomplexation efficiency toward diverse Cu-ligand complexes and a real anodizing effluent, thereby substantiating its practical applicability in wastewater treatment. Mechanistic investigations revealed a biphasic decomplexation pathway under EDTA-abundant conditions: (i) an induction phase wherein MnO_2 generated via alkaline precipitation of Mn^{2+} was oxidized by PMS to produce Mn(V/VI), oxidizing Cu(II) to Cu(III) to trigger rapid ligand oxidation via intramolecular electron abstraction; and (ii) a rapid decomplexation phase wherein decomplexation-liberated Cu^{2+} underwent in-situ transformation into catalytically active CuO nanoparticles. These nanostructures exhibited superior activation capacity to PMS, yielding $^1O_2$ and Cu(III) species that synergistically drove ligand mineralization while enabling concurrent copper immobilization as CuO. This work establishes the Mn(II)/PMS process as an efficient method for Cu(II)-ligand complexes elimination, addressing the critical yet often overlooked issue of ligand interference in practical treatment of industrial wastewater containing Cu(II)-ligand complexes.

Environmental implication

Copper complex-laden wastewater from electroplating, electronics manufacturing, and metal processing industries often contains excessive ligands, which not only passivate added catalysts but also strongly retard the self-enhanced decomplexation effect, leading to inefficient treatment by conventional methods—a challenge that requires reliable solutions. The Mn(II)/PMS system, as a green and efficient approach, addresses this issue by triggering self-enhanced decomplexation effects in both ligand-excess and ligand-deficient environments, offering a robust solution for treating copper complex-laden wastewater. Furthermore, our discovery of synergistic interactions between complexed copper and manganese provides valuable insights for designing future catalytic oxidation systems involving these elements.

CRediT authorship contribution statement

Chengfeng Liu: Investigation. **Jiantong Zhou:** Investigation. **Zhe Xu:** Writing – review & editing, Validation, Supervision, Methodology, Conceptualization. **Weilan Zhen:** Writing – original draft, Validation, Investigation. **Taicheng An:** Writing – review & editing.

Declaration of Competing Interest

The authors declare no competing interests.

Acknowledgements

Financial support from the General Program of the National Natural Science Foundation of China (No. 22176130), the General Program of Guangdong Provincial Natural Science Foundation (No. 2023A1515010906), and the Qihang Program of Guangzhou Natural Science Foundation (No. 2025A04J3817) are gratefully acknowledged.

Appendix A. Supporting information

Supplementary data associated with this article can be found in the online version at doi:10.1016/j.jhazmat.2026.141833.

Data availability

Data will be made available on request.

References

[1] Jiang, K., Zhang, J., Xu, B., Han, Z., Wang, Z., Li, Z., et al., 2025. Selective removal and utilization of copper from electroplating wastewater by modified MXene-based capacitive deionization. Sep Purif Technol 363, 132303. https://doi.org/10.1016/j.seppur.2025.132303.

[2] Dou, W., Peng, X., Kong, L., Xingyun, H., 2022. Removal of Cu(II) and Cu(I) from acidic copper etching wastewater by $NH_3{\cdot}H_2O$ decomplexation coupling with O_2 oxidation. Sep Purif Technol 285, 120348. https://doi.org/10.1016/j.seppur.2021.120348.

[3] Ge, F., Li, M.M., Ye, H., Zhao, B.X., 2012. Effective removal of heavy metal ions Cd^{2+}, Zn^{2+}, Pb^{2+}, Cu^{2+} from aqueous solution by polymer-modified magnetic nanoparticles. J Hazard Mater 211, 366–372. https://doi.org/10.1016/j.jhazmat.2011.12.013.

[4] Zou, Y.R., Wu, S.K., Xu, X.L., Tan, X.Q., Yang, S., Chen, T.T., et al., 2024. Cope with copper: from molecular mechanisms of cuproptosis to copper-related kidney diseases. Int Immunopharmacol 133, 112075. https://doi.org/10.1016/j.intimp.2024.112075.

[5] Lv, S., Zhang, L.H., Zhang, L.F., Liu, S., Fan, W.H., 2025. Hydrogen-producing nanosilicon gel spheres for remediation of copper-polluted aquatic ecosystems: oxidative stress mitigation and ecological recovery. Chem Eng J 504, 159083. https://doi.org/10.1016/j.cej.2024.159083.

[6] Xu, Z., Zhang, Q.R., Li, X.C., Huang, X.F., 2022. A critical review on chemical analysis of heavy metal complexes in water/wastewater and the mechanism of treatment methods. Chem Eng J 429, 131688. https://doi.org/10.1016/j.cej.2021.131688.

[7] Zhu, Y., Fan, W.H., Zhou, T.T., Li, X.M., 2019. Removal of chelated heavy metals from aqueous solution: a review of current methods and mechanisms. Sci Total Environ 678, 253–266. https://doi.org/10.1016/j.scitotenv.2019.04.416.

[8] Du, J.Q., Zhang, B.G., Li, J.X., Lai, B., 2020. Decontamination of heavy metal complexes by advanced oxidation processes: a review. Chin Chem Lett 31 (10), 2575–2582. https://doi.org/10.1016/j.cclet.2020.07.050.

[9] Xu, Z., Gao, G.D., Pan, B.C., Zhang, W.M., Lv, L., 2015. A new combined process for efficient removal of Cu(II) organic complexes from wastewater: Fe(III) displacement/UV degradation/alkaline precipitation. Water Res 87, 378–384. https://doi.org/10.1016/j.watres.2015.09.025.

[10] Huang, X.F., Xu, Y., Shan, C., Li, X.C., Zhang, W.M., Pan, B.C., 2016. Coupled Cu(II)-EDTA degradation and Cu(II) removal from acidic wastewater by ozonation: performance, products and pathways. Chem Eng J 299, 23–29. https://doi.org/10.1016/j.cej.2016.04.044.

[11] Wu, P.X., Zhou, J.B., Wang, X.R., Dai, Y.P., Dang, Z., Zhu, N.W., et al., 2011. Adsorption of Cu-EDTA complexes from aqueous solutions by polymeric Fe/Zr pillared montmorillonite: behaviors and mechanisms. Desalination 277 (1-3), 288–295. https://doi.org/10.1016/j.desal.2011.04.043.

[12] Pan, M.L., Zhang, C., Wang, J., Chew, J.W., Gao, G.D., Pan, B.C., 2019. Multifunctional piezoelectric heterostructure of $BaTiO_3$@graphene: decomplexation of Cu-EDTA and recovery of Cu. Environ Sci Technol 53 (14), 8342–8351. https://doi.org/10.1021/acs.est.9b02355.

[13] Song, Y., Sun, T.R., Cang, L., Wu, S., Zhou, D.M., 2019. Migration and transformation of Cu(II)-EDTA during electrodialysis accompanied by an electrochemical process with different compartment designs. Electrochim Acta 295, 605–614. https://doi.org/10.1016/j.electacta.2018.10.162.

[14] Xu, Z., Wu, T.C., Cao, Y., Chen, C.C., Ke, S.M., Zeng, X.R., et al., 2020. Efficient decomplexation of heavy metal-EDTA complexes by Co^{2+}/peroxymonosulfate process: the critical role of replacement mechanism. Chem Eng J 392, 123639. https://doi.org/10.1016/j.cej.2019.123639.

[15] Liu, Y., Wang, D.F., Xue, M.M., Song, R.Y., Zhang, Y., Qu, G.Z., et al., 2021. High-efficient decomplexation of Cu-EDTA and Cu removal by high-frequency non-thermal plasma oxidation/alkaline precipitation. Sep Purif Technol 257, 117885. https://doi.org/10.1016/j.seppur.2020.117885.

[16] Kan, H.S., Mao, R., Zhu, X., Cui, Y.X., Liu, Y., Wang, K.F., et al., 2024. Self-catalytic decomplexation of Cu-TEPA and simultaneous recovery of Cu by an electrochemical ozone production system using heterojunction Ni-Sb-SnO_2 anode. J Hazard Mater 465, 132967. https://doi.org/10.1016/j.jhazmat.2023.132967.

[17] Kan, H.S., Mao, R., Pu, H., Cui, Y.X., Liu, Y., Zhao, X., 2025. Targeted tuning of heterojunction anode in electrochemical ozone production process for boosting self-catalytic heavy metal complex decomplexation and metal recovery. Appl Catal BEnviron Energy 370, 125178. https://doi.org/10.1016/j.apcatb.2025.125178.

[18] Zu, D.Y., Song, H.R., Li, C.P., Wang, Y.W., Du, R., Zhou, R., et al., 2022. Understanding the self-catalyzed decomplexation mechanism of Cu-EDTA in $Ti_3C_2T_x$ MXene/peroxymonosulfate process. Appl Catal BEnviron Energy 306, 121131. https://doi.org/10.1016/j.apcatb.2022.121131.

[19] Lan, S.Y., Xiong, Y., Tian, S.H., Feng, J.X., Xie, T.Y., 2016. Enhanced self-catalytic degradation of CuEDTA in the presence of H_2O_2/UV: evidence and importance of Cu-peroxide as a photo-active intermediate. Appl Catal BEnviron 183, 371–376. https://doi.org/10.1016/j.apcatb.2015.10.030.

[20] Liu, Y., Lu, M.Q., Yin, Y.R., Zhou, J., Qu, G.Z., Zhang, Y., et al., 2022. Self-catalytic Fenton-like reactions stimulated synergistic Cu-EDTA decomplexation and Cu recovery by glow plasma electrolysis. Chem Eng J 433. https://doi.org/10.1016/j.cej.2022.134601.

[21] Xu, Z., Shan, C., Xie, B.H., Liu, Y., Pan, B.C., 2017. Decomplexation of Cu(II)-EDTA by UV/persulfate and UV/H_2O_2: efficiency and mechanism. Appl Catal BEnviron 200, 439–447. https://doi.org/10.1016/j.apcatb.2016.07.023.

[22] Huang, X.F., Wan, Y., Li, X.C., Guan, D.X., Li, Y.B., Zheng, X.Y., et al., 2019. Autocatalytic decomplexation of Cu(II)-EDTA and simultaneous removal of aqueous Cu(II) by UV/chlorine. Environ Sci Technol 53 (4), 2036–2044. https://doi.org/10.1021/acs.est.8b05346.

[23] Li, J.Y., Ma, J.X., Dai, R.B., Wang, X.Y., Chen, M., Waite, T.D., et al., 2021. Self-enhanced decomplexation of Cu-organic complexes and Cu recovery from wastewaters using an electrochemical membrane filtration system. Environ Sci Technol 55 (1), 655–664. https://doi.org/10.1021/acs.est.0c05554.

[24] Mu, Y., Tong, X.L., Guan, Y.Y., Yu, Q.H., Ren, W., Tian, L., et al., 2025. Simultaneous copper and EDTA ligands recovery from electroless effluent with metallic copper and formaldehyde. Environ Sci Technol 59 (1), 968–977. https://doi.org/10.1021/acs.est.4c09970.

[25] Yu, J.Y., Deng, W., Huang, X.F., Zhao, M., Li, X.C., Zhang, T., et al., 2024. Intramolecular generation of endogenous Cu(III) for selectively self-catalytic degradation of Cu(II)-EDTA from wastewater by UV/peroxymonosulfate. J Hazard Mater 465, 133521. https://doi.org/10.1016/j.jhazmat.2024.133521.

[26] Chu, Z., Han, Z., Liu, H., Chen, T., Zou, X., Wang, H., et al., 2024. Autocatalytic degradation of Cu-EDTA in the calcite/PMS system: singlet oxygen and Cu(III). J Hazard Mater 477, 135286. https://doi.org/10.1016/j.jhazmat.2024.135286.

[27] Chen, Y., Mu, Y., Tian, L., Zheng, L.L., Mei, Y., Xing, Q.J., et al., 2023. Targeted decomplexation of metal complexes for efficient metal recovery by ozone/percarbonate. Environ Sci Technol 57 (12), 5034–5045. https://doi.org/10.1021/acs.est.3c00190.

[28] Wang, L., Xu, H., Jiang, N., Wang, Z., Jiang, J., Zhang, T., 2020. Trace cupric species triggered decomposition of peroxymonosulfate and degradation of organic pollutants: Cu(III) being the primary and selective intermediate oxidant. Environ Sci Technol 54 (7), 4686–4694. https://doi.org/10.1021/acs.est.0c00284.

[29] Gao, Y., Zhou, Y., Pang, S.Y., Jiang, J., Shen, Y.M., Song, Y., et al., 2021. Enhanced peroxymonosulfate activation via complexed Mn(II): a novel non-radical oxidation mechanism involving manganese intermediates. Water Res 193, 116856. https://doi.org/10.1016/j.watres.2021.116856.

[30] Gong, C., Chen, F., Yang, Q., Luo, K., Yao, F.B., Wang, S.N., et al., 2017. Heterogeneous activation of peroxymonosulfate by Fe-Co layered doubled hydroxide for efficient catalytic degradation of Rhoadmine B. Chem Eng J 321, 222–232. https://doi.org/10.1016/j.cej.2017.03.117.

[31] Sun, S., Shan, C., Yang, Z., Wang, S., Pan, B., 2022. Self-enhanced selective oxidation of phosphonate into phosphate by Cu(II)/H_2O_2: Performance, mechanism, and validation. Environ Sci Technol 56 (1), 634–641. https://doi.org/10.1021/acs.est.1c06471.

[32] Liu, W.F., Sun, B., Qiao, J.L., Guan, X.H., 2019. Influence of pyrophosphate on the generation of soluble Mn(III) from reactions involving Mn oxides and Mn(VII). Environ Sci Technol 53 (17), 10227–10235. https://doi.org/10.1021/acs.est.9b03456.

[33] Shi, Y.F., Xiao, S.Z., Qian, Y.J., Huang, C.H., Chen, J.B., Li, N., et al., 2024. Revisiting the synergistic oxidation of peracetic acid and permanganate (VII) towards micropollutants: the enhanced electron transfer mechanism of reactive manganese species. Water Res 262, 122105. https://doi.org/10.1016/j.watres.2024.122105.

[34] Yang, T., Mai, J.M., Zhu, M.Y., Peng, Q.Q., Huang, C., Wu, S.S., et al., 2022. Enhanced permanganate activation under UVA-LED irradiation: unraveled mechanism involving manganese species and hydroxyl radical. Environ Sci Technol 56 (24), 17720–17731. https://doi.org/10.1021/acs.est.2c06290.

[35] Yang, Y., Jiang, J., Lu, X.L., Ma, J., Liu, Y.Z., 2015. Production of sulfate radical and hydroxyl radical by reaction of ozone with peroxymonosulfate: a novel advanced oxidation process. Environ Sci Technol 49 (12), 7330–7339. https://doi.org/10.1021/es506362e.

[36] Ball, Donald L., Edwards, John O., 1956. The kinetics and mechanism of the decomposition of Caro's acid. J Am Chem Soc 78 (6), 1125–1129. https://doi.org/10.1021/ja01587a011.

[37] Zhou, Y., Jiang, J., Gao, Y., Ma, J., Pang, S.Y., Li, J., et al., 2015. Activation of peroxymonosulfate by benzoquinone: a novel nonradical oxidation process. Environ Sci Technol 49 (21), 12941–12950. https://doi.org/10.1021/acs.est.5b03595.

[38] Huang, W.Y., Brigante, M., Wu, F., Mousty, C., Hanna, K., Mailhot, G., 2013. Assessment of the Fe(III)-EDDS complex in Fenton-like processes: from the radical formation to the degradation of bisphenol A. Environ Sci Technol 47 (4), 1952–1959. https://doi.org/10.1021/es304502y.

[39] Chen, J., Sun, B., Zhu, Y.T., Yang, Y.Q., Guan, X.H., 2022. Unraveling the role of Mn(VI) and Mn(V) species in contaminant abatement by permanganate. Environ Sci Technol Lett 9 (5), 446–451. https://doi.org/10.1021/acs.estlett.2c00165.

[40] Klewicki, J.K., Morgan, J.J., 1998. Kinetic behavior of Mn(III) complexes of pyrophosphate, EDTA, and citrate. Environ Sci Technol 32 (19), 2916–2922. https://doi.org/10.1021/es980308e.

[41] Wang, Y., Qiu, W., Lu, X., Zhou, X., Zhang, H., Gong, X., et al., 2023. Nitrilotriacetic acid-assisted Mn(II) activated periodate for rapid and long-lasting

degradation of carbamazepine: the importance of Mn(IV)-oxo species. Water Res 241, 120156. https://doi.org/10.1016/j.watres.2023.120156.

[42] Zheng, M.W., Lin, C.W., Chou, P.H., Chiang, C.L., Lin, Y.G., Liu, S.H., 2024. Highly effective degradation of ibuprofen by alkaline metal-doped copper oxides via peroxymonosulfate activation: mechanisms, degradation pathway and toxicity assessments. J Hazard Mater 462, 132751. https://doi.org/10.1016/j.jhazmat.2023.132751.

[43] Shan, C., Xu, Z., Zhang, X.L., Xu, Y., Gao, G.D., Pan, B.C., 2018. Efficient removal of EDTA-complexed Cu(II) by a combined Fe(III)/UV/alkaline precipitation process: performance and role of Fe(II). Chemosphere 193, 1235–1242. https://doi.org/10.1016/j.chemosphere.2017.10.119.